Expected constraints on the generalized Chaplygin equation of state from future supernova experiments and gravitational lensing statistics.

P.T. Silva

`paptms@ist.utl.pt`

and

O. Bertolami

`orfeu@cosmos.ist.utl.pt`

Instituto Superior Técnico, Departamento de Física.
Av. Rovisco Pais 1, 1049-001 Lisboa, Portugal

ABSTRACT

This paper aims to study the use of future SNAP data together with the result of searches for strong gravitational lenses in future large quasar surveys to constrain the Generalized Chaplygin Gas (GCG) model, with equation of state $p = -A/\rho^{\alpha}$, where A is a positive constant and $0 < \alpha \leq 1$. The GCG is considered as a possible unification scheme for dark matter-dark energy. It is found that both experiments should be able to place important constraints on the model, especially when both tests are used together.

Subject headings: cosmology: cosmological parameters, dark matter — equation of state — gravitational lensing

1. Introduction

In the last few years there has been mounting evidence that not only visible matter is a small component of the observable Universe, but that matter itself, dark or visible, makes up only a fraction of the cosmic energy budget. Indeed, SNe Ia experiments indicate that the Universe is expanding in an accelerated fashion (Riess et al. 1998; Garnavich et al.

arXiv:astro-ph/0303353v2 3 Jul 2003

1998; Perlmutter et al. 1999), and together with nucleosynthesis constraints (Burles, Nollet, & Turner 2001), and the CMBR power spectrum (Balbi et al. 2000; de Bernardis et al. 2000; Jaffe et al. 2001) it is possible to arrive to a concordance where the Universe is made of about 5% of baryonic matter, 25% of dark matter and 70% of dark energy, a negative pressure component. These results are also in agreement with large scale structure (Peacock et al. 2001), and independent determinations of the matter density (Bachall & Fan 1998; Carlberg et al. 1998; Turner 2000). The nature of the dark matter and of the dark energy is not well established; dark matter candidates include axions, neutralinos and possibly a self-interacting scalar-field (see e.g. Bento, Bertolami, & Rosenfeld 2001 and references therein), while the most obvious candidate for the dark energy is the vacuum energy, or an uncanceled cosmological constant (Bento & Bertolami 1999; Bento, Bertolami, & Silva 2001). Another possibility is a dynamical vacuum (Bronstein 1933; Bertolami 1986a,b; Ozer & Taha 1987) or quintessence. Quintessence models most often involve a single scalar field (Ratra & Peebles 1988a,b; Wetterich 1988; Caldwell, Dave, & Steinhardt 1998; Ferreira & Joyce 1998; Zlatev, Wang, & Steinhardt 1999; Binétruy 1999; Kim 1999; Uzan 1999; Amendola 1999; Albrecht & Skordis 2000; Bertolami & Martins 2000; Banerjee & Pavón 2001a,b; Sen & Sen 2001; Sen, Sen, & Sethi 2001) or two coupled fields (Fujii 2000; Masiero, Pietroni, & Rosati 2000; Bento, Bertolami, & Santos 2002). However, these models are afflicted with a fine tuning problem to explain the cosmic coincidence problem, that is, why did the dark energy start to dominate the cosmological evolution only fairly recently.

Recently a new possibility has been suggested in Kamenshchik, Moschella, & Pasquier (2001), Bilić, Tupper, & Viollier (2002), and Bento, Bertolami, & Sen (2002a), which uses an exotic equation of state, and considers the evolution of the equation of state of the background fluid instead of a quintessence potential. This is achieved by using a background fluid, the generalized Chaplygin gas (GCG), described by the equation of state (Kamenshchik, Moschella, & Pasquier 2001; Bento et al. 2002a)

$$p_{ch} = -\frac{A}{\rho_{ch}^{\alpha}} \ . \tag{1}$$

The case $\alpha = 1$ is called the Chaplygin equation of state, $p_{ch} = -A/\rho_{ch}$, while when $\alpha = 0$, the model behaves as the flat ΛCDM, as discussed in Section II. The quantity A is related to the present day Chaplygin adiabatic sound speed through $v_s^2 = \alpha A/\rho_{ch,0}$, where $\rho_{ch,0}$ is the GCG density at present. This model allows for an unification of dark energy and dark matter and admits a brane interpretation (Bento et al. 2002a). Furthermore, analyses indicate that it may be accommodated within the standard structure formation scenario (Bilić et al. 2002; Bento et al. 2002a). These results have been challenged in Sandvik et al. (2002), however their analysis does not take into account the effect of baryons, which is expected and shown to be important (Beça et al. 2003), and makes the GCG model compatible with the 2DF

mass power spectrum. Also, Sandvik et al. (2002) analysis is based on the linear treatment of pertubations close to the present time, thus neglecting any non-linear effects. Thus we consider that a more careful and thorough analysis must be done before ruling out the GCG model on the grounds of its effects in the matter power spectrum or structure formation.

Since the GCG exhibited great potentialities, it has been recently the subject of great interest, and various attempts have been made to constrain the model using the available observational data. In Avelino et al. (2002) the GCG was tested against the SNe Ia data and the matter power spectrum, and it is concluded that the GCG model agrees with the data, and interesting constraints on $A_s = A/\rho_{ch,0}^{1+\alpha}$ are found for fixed values of α. Also, the value $A_s = 1$, corresponding to a pure cosmological constant, is strongly ruled out by data. The limits were somewhat degenerate mainly because three parameters, α, A_s, and the density relative to critical of the Chaplygin gas, Ω_{ch}, were considered. In Dev, Alcaniz, & Jain (2002) tests on the age of the Universe and strong lensing statistics were used to constrain the Chaplygin equation of state ($\alpha = 1$), and it is found that the available data agrees with a Chaplygin gas model; from the age test it is concluded that $A_s \geq 0.96$, and from the statistics of lensed quasars it is concluded that $A_s \geq 0.72$. The age test together with SNe distance measurements were used to constrain the generalized Chaplygin equation of state in a flat Universe made up of the GCG and baryons, with fixed densities relative to critical, yielding confidence regions in the $(A_s; \alpha)$ plane (Makler, Oliveira & Waga 2002). The data indicated that $0.6 \lesssim A_s \lesssim 0.85$ at 95% confidence level (CL) and almost no constraints of interest to parameter α. The strongest constraints were obtained by Bento et al. (2002b) using the CMBR power spectrum measurements from BOOMERANG (de Bernardis et al. 2002) and Archeops (Benoit et al. 2002), together with the SNe Ia constraints from Makler et al. (2002). It is found that $0.74 \lesssim A_s \lesssim 0.85$, and $\alpha \lesssim 0.6$, ruling out the pure Chaplygin gas model. Using the bound arising from the age of the APM 08279+5255 source, which is $A_s \gtrsim 0.81$ (Alcaniz, Jain, & Dev 2002), fairly tight constraints are found, namely $0.81 \lesssim A_s \lesssim 0.85$, and $0.2 \lesssim \alpha \lesssim 0.6$, which also rules out the ΛCDM model. These results were found to agree with the WMAP data (Bento et al. 2003).

The prospect of launching the SNAP satellite[1] will give rise to a new era of precision cosmology, and together with data from CMBR experiments and from large quasar and galaxy surveys, cosmologists will be able to test several models with unprecedented accuracy. Of course, this increase in accuracy may find its limits in new degeneracies, given the growth of free parameters, which in turn will require the use of more cosmological tests to distinguish competing models. In this paper we aim to study how well the GCG model can be constrained

---

[1]snap.lbl.gov

with future data from the SNAP satellite, and from strong lensing statistics. We will be especially interested in the use of the Sloan Digital Sky Survey[2] (SDSS) data to constrain cosmological parameters, and also smaller surveys such as the 2dF[3]. Even though it has already been verified that the SNAP satellite will be able to constrain the model quite accurately (Avelino et al. 2002; Makler et al. 2002), the tighter constraints provided by the CMBR (Bento et al. 2002b, 2003) invite us to go a step forward as SNe confidence regions depend strongly on the fiducial model considered. Moreover, we add that the use of gravitational lensing statistics from future large surveys has not been explored in the context of the Chaplygin gas. Thus, the main aim of the our study is to use all three tests to constrain as much as possible the parameters of the GCG.

The outline of this paper is as follows. In Section 2 we explain how the Chaplygin model closely mimics the ΛCDM model, and show that the case $\alpha = 0$ corresponds to the ΛCDM model. In Section 3 we consider the magnitude versus redshift cosmological test. In 3.1 we briefly describe the nature of this test, and in 3.2 we estimate the errors considered. In 3.3 we describe the method used to obtain the confidence regions shown in 3.4.

Section 4 is dedicated to strong lensing statistics. In 4.1 we briefly describe the strong lensing test, in 4.3 we explain how we use the Fisher matrix formalism to build the confidence regions that are exhibited in 4.4.

2. Generalized Chaplygin gas compared to flat ΛCDM.

The cosmological tests considered here depend on the cosmological model through the comoving distance $r(z, H_0, \mathbf{\Theta})$, where $\mathbf{\Theta}$ is a vector containing the cosmological parameters we are interested in determining, and H_0 being the Hubble constant. For a Friedman-Robertson-Walker (FRW) Universe the comoving distance as function of redshift is given by

$$
r(z, H_0, \Theta) = \begin{cases} \dfrac{c}{H_0\sqrt{-\Omega_k}} \sin\left(\displaystyle\int_0^z \dfrac{H_0\sqrt{-\Omega_k}dz'}{H(z', H_0, \Theta)}\right) & \Omega_k < 0 \\[3ex] c\displaystyle\int_0^z \dfrac{dz'}{H(z', H_0, \Theta)} & \Omega_k = 0 \\[3ex] \dfrac{c}{H_0\sqrt{\Omega_k}} \sinh\left(\displaystyle\int_0^z \dfrac{H_0\sqrt{\Omega_k}dz'}{H(z', H_0, \Theta)}\right) & \Omega_k > 0 \end{cases} \tag{2}
$$

---

[2]www.sdss.org

[3]www.2dfquasar.org

where $\Omega_k = 1 - \Omega$, Ω being the total density of the Universe relative to the critical one. Only flat cosmological models, $\Omega_k = 0$, are considered in this paper.

The expansion rate may be written in terms of the total mass-energy density as a function of redshift. Recalling the Friedman equation,

$$H^2(z) = \frac{8\pi G}{3}\rho(z) , \qquad (3)$$

where $\rho(z)$ is the total mass-energy density at redshift z, the expansion rate is given by

$$H(z) = H_0 \left(\frac{\rho(z)}{\rho_0}\right)^{1/2} , \qquad (4)$$

where $\rho_0 = \rho(0)$ is the energy density at present. For a flat Universe, $\rho_0 = \rho_c$, where ρ_c is the critical density.

For the flat ΛCDM, ignoring the small radiation energy density contribution, one has

$$\rho(z) = \rho_0 \left[\Omega_\Lambda + (\Omega_{CDM} + \Omega_b)(1 + z)^3\right] , \qquad (5)$$

where Ω_b, Ω_{CDM}, Ω_Λ are the baryonic, cold dark matter and vacuum energy densities relative to critical, respectively. Thus, the Hubble parameter becomes

$$H(z) = H_0 \left[\Omega_\Lambda + (\Omega_{CDM} + \Omega_b)(1 + z)^3\right]^{1/2} . \qquad (6)$$

The GCG unifies dark matter and energy, but does not account for the baryons. Therefore in a consistent model of the Universe baryons and radiation must be included. The contribution of radiation shall be ignored, since its effect is not important for the redshifts considered here. Hence, for a Universe made up of the GCG plus baryons one has (Bento et al. 2002a)

$$\rho_{ch}(z) = \rho_{b,0}(1 + z)^3 + \left(A + B(1 + z)^{3(1+\alpha)}\right)^{1/(1+\alpha)} . \qquad (7)$$

where $\rho_{b,0}$ is the baryon density at present, and B is an integration constant. Using the freedom to define the integration constant B, this expression may be rewritten as

$$\rho_{ch}(z) = \rho_{b,0}(1 + z)^3 + \rho_{ch,0}\left[A_s + (1 - A_s)(1 + z)^{3(1+\alpha)}\right]^{1/(1+\alpha)} , \qquad (8)$$

where $\rho_{ch,0} = (A + B)^{1/(1+\alpha)}$ is the present day density of the Chaplygin gas, and $A_s \equiv A/\rho_{ch,0}^{1+\alpha}$. Thus, for a flat Universe, the Friedman equation becomes

$$H_{ch}(z) = H_0 \left\{\Omega_b(1 + z)^3 + \Omega_{ch}\left[A_s + (1 - A_s)(1 + z)^{3(1+\alpha)}\right]^{1/(1+\alpha)}\right\}^{1/2} , \qquad (9)$$

where $\Omega_{ch} = \rho_{ch,0}/\rho_c$ is the GCG density relative to the critical one.

Even though the generalized Chaplygin equation of state looks rather exotic, the resulting cosmological model behaves in a manner that mimics the ΛCDM model (Bento et al. 2002a). First let us consider the very early Universe, when its size was very small compared to the present one, $a(z) \ll a_0 \equiv 1$, or $z \gg 0$. The ΛCDM behaves as a flat CDM dominated Universe:

$$\rho(z \gg 0) = \rho_0 \left(\Omega_{CDM} + \Omega_b \right) (1 + z)^3 . \tag{10}$$

The GCG also behaves as a flat CDM dominated Universe with a dark matter density $\Omega_{CDM} = \Omega_{ch}(1 - A_s)^{1/(1+\alpha)}$, as may be seen in

$$\rho_{ch}(z \gg 0) = \rho_0 \left(\Omega_b + \Omega_{ch}(1 - A_s)^{1/(1+\alpha)} \right) (1 + z)^3 . \tag{11}$$

This property ensures that the GCG model is consistent, at large scales, with the CDM structure formation scenario.

Consider now the late Universe, when $a \gg a_0$. The ΛCDM behaves as a vacuum dominated Universe,

$$\rho(a \gg a_0) = \rho_0 \Omega_\Lambda , \tag{12}$$

while the GCG model also behaves as a vacuum dominated Universe, that at present has a vacuum density $\Omega_\Lambda = \Omega_{ch} A_s^{1/(1+\alpha)}$,

$$\rho_{ch}(a \gg a_0) = \rho_0 \Omega_{ch} A_s^{1/(1+\alpha)} . \tag{13}$$

Between these two limits, the GCG density may be expanded in subleading terms, yielding

$$\rho_{ch} = \rho_0 \left\{ \Omega_b(1 + z)^3 + \Omega_{ch} \left[A_s^{1/(1+\alpha)} + \frac{1}{1 + \alpha} \frac{1 - A_s}{A_s^{\alpha/(1+\alpha)}} (1 + z)^{3(1+\alpha)} \right] \right\} . \tag{14}$$

Thus, between the dust and the De Sitter phases, the GCG behaves like a two component fluid made up of vacuum energy with a present day density given by $\Omega_\Lambda = \Omega_{ch} A_s^{1/(1+\alpha)}$, and soft matter with the equation of state $\rho = \alpha p$, and at present

$$\Omega_{sm} = \Omega_{ch} \left(\frac{1}{1 + \alpha} \right) \frac{1 - A_s}{A_s^{\alpha/(1+\alpha)}} . \tag{15}$$

Also, making the associations

$$\begin{aligned}
\Omega_{ch}^{1+\alpha} A_s &\quad \rightarrow \quad \Omega_\Lambda^{1+\alpha} , \\
\Omega_{ch}^{1+\alpha}(1 - A_s) &\quad \rightarrow \quad \Omega_{CDM}^{1+\alpha} ,
\end{aligned} \tag{16}$$

and using them in Eqs. (8-9), one obtains

$$\rho_{ch}(z) \quad = \quad \rho_{b,0}(1+z)^3 + \rho_0 \left[\Omega_\Lambda^{1+\alpha} + \Omega_{CDM}^{1+\alpha}(1+z)^{3(1+\alpha)}\right]^{1/(1+\alpha)} , \tag{17}$$

$$H_{ch}(z) \quad = \quad H_0 \left\{\Omega_b(1+z)^3 + \left[\Omega_\Lambda^{1+\alpha} + \Omega_{CDM}^{1+\alpha}(1+z)^{3(1+\alpha)}\right]^{1/(1+\alpha)}\right\}^{1/2} , \tag{18}$$

$$\left[\Omega_\Lambda^{1+\alpha} + \Omega_{CDM}^{1+\alpha}\right]^{1/(1+\alpha)} + \Omega_b = 1 , \tag{19}$$

which allows one to see that $\alpha = 0$ is identical to the flat ΛCDM model.

3. Magnitude versus redshift cosmological test.

3.1. Description of the test.

The magnitude versus redshift test explores the dependence of the distance modulus of a source on its redshift. For a source with redshift z, its apparent magnitude is related to its absolute magnitude through

$$m(z) = M + 5 \log d_L(z, H_0, \boldsymbol{\Theta}) + 25 , \tag{20}$$

where $\boldsymbol{\Theta}$ represents the several cosmological parameters we are interested in, d_L is the luminosity distance, $d_L = (1+z)r$, measured in units of 10 pc, and r is the comoving distance, Eq. (2). The luminosity distance is then given by

$$d_L(z, H_0, \Theta) = \begin{cases} \dfrac{(1+z)c}{H_0\sqrt{-\Omega_k}} \sin\left(\displaystyle\int_0^z \dfrac{H_0\sqrt{-\Omega_k}dz'}{H(z', H_0, \Theta)}\right) & \Omega_k < 0 , \\[3ex] (1+z)c \displaystyle\int_0^z \dfrac{dz'}{H(z', H_0, \Theta)} & \Omega_k = 0 , \\[3ex] \dfrac{(1+z)c}{H_0\sqrt{\Omega_k}} \sinh\left(\displaystyle\int_0^z \dfrac{H_0\sqrt{\Omega_k}dz'}{H(z', H_0, \Theta)}\right) & \Omega_k > 0 . \end{cases} \tag{21}$$

Defining a new quantity $D_L = H_0 d_L$ one may group the terms that depend on the absolute magnitude and H_0. The apparent magnitude then reads

$$\begin{aligned} m(z, H_0, \Theta) \quad &= \quad M - 5\log(H_0) + 25 - 5\log D_L(z, \Theta) \\ &= \quad \mathcal{M} - 5\log D_L(z, \Theta) . \end{aligned} \tag{22}$$

The quantity $\mathcal{M} = M - 5\log H_0 + 25$ is usually called zero point value or *intercept* since it it the value of the apparent magnitude at the point where $\log D_L = 0$. This quantity can be

measured using low redshift SNe, or be treated as a statistical nuisance that is marginalized (Permutter et al. 1997). We shall follow Goliath et al. (2001) and assume either an exact knowledge of $\mathcal{M}$ or no prior knowledge of it. This allows us to concentrate on the study of the parameters that are relevant to us.

3.2. Error estimates for one year of SNAP data.

In the next subsections we aim to study the ability of the SNAP mission to test the GCG equation of state. We shall use the expected error estimates for the SNAP satellite from Weller & Albrecht (2002), and consider that the systematic errors for the aparent magnitude m are given by

$$\sigma_{sys}(z) = \frac{0.02}{1.5}z \ , \tag{23}$$

which are measured in magnitudes such that at $z = 1.5$ the systematic error is 0.02 magnitudes, while the statistical errors for m are estimated to be $\sigma_{sta} = 0.15$ magnitudes. We place the SNe in bins of width $\Delta z \approx 0.05$. We then sum both kind of errors quadratically

$$\sigma_{mag}(z_i) = \sqrt{\sigma_{sys}^2(z_i) + \frac{\sigma_{sta}^2}{n_i}} \ , \tag{24}$$

where n_i is the number of supernovae in the redshift bin. The distribution of supernovae in each redshift bin is the same considered in Weller & Albrecht (2002), and is shown in Table 1.

3.3. Confidence regions for SNe Ia tests.

To build the confidence regions a fiducial model corresponding to a vector $\mathbf{\Theta}_{true}$ is chosen, and log-likelihood functions χ^2 are calculated based on hypothetical magnitude measurements at the various redshifts. This function is given by

$$\chi^2(\mathcal{M}, \mathbf{\Theta}) = \sum_{z_i=0}^{z_{max}} \frac{[m(z, \mathcal{M}, \mathbf{\Theta}) - m(z, \mathcal{M}, \mathbf{\Theta}_{theory})]^2}{\sigma^2(z)} \ , \tag{25}$$

where the sum is made over all redshift bins and $m(z, \mathcal{M}, \mathbf{\Theta})$ is defined as in Eq. (22).

The χ^2 function is directly related to the maximum likelihood estimator of a normal random variable, $L = \exp(-\chi^2/2)$. Suppose one wants to impose a Gaussian prior to one of

the parameters being measured, θ, centered around θ_0, with variance σ_θ^2. Using the Bayes theorem one finds that

$$L = \exp(-\frac{1}{2}\chi^2) \exp\left(\frac{(\theta - \theta_0)^2}{2\sigma_\theta^2}\right) . \tag{26}$$

Thus, the χ^2 function is changed to

$$\chi^2 \to \chi^2 + \frac{(\theta - \theta_0)^2}{\sigma_\theta^2} . \tag{27}$$

If one aims to impose a prior on a given parameter one is not measuring, one has to integrate the parameter out of the likelihood function using its probability density function, $p(\theta)$, as prior, that is

$$\chi^2_{\text{prior on } \theta} = -2\ln \int_{-\infty}^{+\infty} d\theta \exp\left(-\frac{1}{2}\chi^2\right) p(\theta) . \tag{28}$$

A special case is the marginalization over the zero point $\mathcal{M}$. When this zero point is exactly known it cancels out from the χ^2 expression, and the modified log-likelihood function $\hat{\chi}^2$ (Goliath et al. 2001) is obtained,

$$\hat{\chi}^2 = \sum_{i=1}^{n} \frac{\Delta^2}{\sigma_i^2} , \tag{29}$$

where

$$\Delta = 5\log_{10}[D_L(z, \mathbf{\Theta})] - 5\log_{10}[D_L(z, \mathbf{\Theta}_{true})] . \tag{30}$$

Assuming no prior at all about $\mathcal{M}$, one has to integrate it out of the χ^2 function, obtaining a modified log-likelihood function $\widetilde{\chi}^2$:

$$\begin{aligned} \widetilde{\chi}^2 &= -2\ln \int_{-\infty}^{+\infty} d\mathcal{M} \exp\left(-\frac{1}{2}\chi^2\right) \\ &= \hat{\chi}^2 - \frac{B^2}{C} + \ln\left(\frac{C}{2\pi}\right) , \end{aligned} \tag{31}$$

where

$$B = \sum_{i=1}^{n} \frac{\Delta}{\sigma_i^2} , \tag{32}$$

$$C = \sum_{i=1}^{n} \frac{1}{\sigma_i^2} . \tag{33}$$

3.4. Expected Confidence regions for 1 year of SNAP data.

The values used for each fiducial model are shown in Table 2. As mentioned above, the use of SNAP data to constrain the GCG model was already considered in Makler et al. (2002) and Avelino et al. (2002), but our analysis differs these ones in three points. Firstly, the Avelino et al. (2002) analysis is done in the (Ω_{ch}, A_s) plane for fixed values of α, while we consider Ω_{ch} fixed, and find constraints in the (A_s, α) plane. Secondly, in Makler et al. (2002) only a ΛCDM fiducial model is considered, essentially with the purpose of testing whether SNAP will be able to rule out the GCG model, noting that it will be possible to distinguish between a ΛCDM and the Chaplygin gas ($\alpha = 1$) model. Our analysis not only considers the capability of ruling out the GCG model, via our study of Model I, but also considers the precision of the constrains one may find for both our fiducial models. The inclusion of this second fiducial model is important, as it corresponds to the center point of the range allowed by CMBR (Bento et al. 2002b) and the age test (Alcaniz et al. 2002). Thirdly, we are not only interested in the use of SNAP to constrain the model, but also the use of strong gravitational lensing statistics, and especially to study what constraints might arise when both probes are used together. Throughout the paper we will also use the CMBR constraints from Bento et al. (2002b), essentially with two purposes. Firstly to compare these available constraints with the future ones, to see whether future tests will be able to improve the available constrains or merely confirm them, and secondly as a third test that might be used to improve the confidence regions.

The expected confidence regions that are obtained are shown in Figures 1-3. In all cases a fixed baryon density with value $\Omega_b = 0.05$ is used. Two fiducial models were considered. Model I corresponds to the center value of the parameter range found by Bento et al. (2002b), $(A_s, \alpha) = (0.83, 0.4)$. Model II corresponds to a flat ΛCDM model with $\Omega_\Lambda = 0.72$, $\Omega_{CDM} = 0.23$, and $\Omega_b = 0.05$. Using the associations given in section 3.1, this corresponds to $(A_s, \alpha) = (0.758, 0)$. Both sets of values are compatible with the CMBR data (Bento et al. 2002b) and available SNIa data (Makler et al. 2002). The set corresponding to the ΛCDM fiducial model is ruled out by the age estimate of the APM 08279-5255 source (Alcaniz et al. 2002), but it was included to illustrate the effect of choosing a fiducial model.

The first conclusion one draws is that in order to achieve some precision, a good estimate of the intercept $\mathcal{M}$ is required. Without imposing prior knowledge of $\mathcal{M}$ it is possible to distinguish only between a ΛCDM model ($\alpha = 0$) and a generalized Chaplygin model with $\alpha \gtrsim 0.75$ at 95% confidence level (CL), or with $\alpha \gtrsim 0.4$ at 68% CL, as shown in Figures 2 and 3. For Model I (Figure 2) the situation is even worse, and without a good knowledge of the intercept it is only possible to distinguish between models with $\alpha \gtrsim 0.9$ at 68% CL. In either case the pure Chaplygin gas ($\alpha = 1$) is ruled out with 68% CL. To distinguish between

both fiducial models a good estimate of $\mathcal{M}$ is necessary.

In the previous paragraph the ability of the test to distinguish between models was considered. Next we consider whether it is possible to improve on the limits imposed by the CMBR (Bento et al. 2002b), available SNe (Makler et al. 2002) and the age test (Alcaniz et al. 2002). We find that the answer depends on the fiducial model considered. For Model II it is possible to confirm or to reject the present limits. Indeed, using CMBR constraints from Bento et al. (2002b), Figure 1, leads to a smaller parameter region, but it allows no more than to assert that $0.2 \lesssim \alpha \lesssim 0.65$ and $0.81 \lesssim A_S \lesssim 0.85$ at 68% CL, or $0.15 \lesssim \alpha \lesssim 0.75$ and $0.79 \lesssim A_S \lesssim 0.87$ at 95% CL.

For Model I, the situation is different. This model is not compatible with the age estimate of the APM 08279-5255 source (Alcaniz et al. 2002), therefore the comparison must be made with the allowed parameter range from available SNe data and the CMBR constraints from Bento et al. (2002b). From only these two tests one can establish that $0.74 \lesssim A_s \lesssim 0.85$, and $0 \lesssim \alpha \lesssim 0.6$ (Bento et al. 2002b; Makler et al. 2002). For this fiducial model, the SNAP data will allow for tighter constraints, yielding $0.75 \lesssim A_S \lesssim 0.80$ and $\alpha \lesssim 0.35$ at 95% CL. The use of additional CMBR constraints from Bento et al. (2002b) will allow further constraining α to $\alpha \lesssim 0.3$ at 95% CL.

4. Strong lensing probability.

4.1. Description of the test.

We start the description of the strong lensing probability test by setting the assumptions which are most commonly used in gravitational lensing statistics, namely:

- Lensing galaxies are described by singular isothermal sphere (SIS) profiles.

- There is no evolution in the population of lensing galaxies.

- The Tully-Fisher and Faber-Jackson relations are independent of redshift.

Under these assumptions, in a flat FRW Universe the probability that a source at redshift z_S will be lensed by a galaxy is given by (Turner, Ostriker, & Gott 1984; Gott, Park, & Lee 1989)

$$\tau = F\frac{r^3(z_S)}{30R_0^3} \, , \tag{34}$$

where $R_0 = c/H_0$, $r(z)$ is the comoving distance, Eq. (2), and F is the dimensionless parameter

$$F = \frac{16\pi^3}{cH_0^3} < n_0\sigma_\parallel^4 > , \tag{35}$$

n_0 being the number density of galaxies at present and $\sigma_\parallel$ is their velocity dispersion. The average is computed over all lensing galaxies using the Tully-Fisher and Faber-Jackson relations together with the galaxy luminosity function (Fukugita & Turner 1991). We shall use the value estimated in Cooray (1999), $F = 0.026$. The information concerning the cosmological model enters through the comoving distance.

4.2. Magnification bias and selection effects.

To sucessfully use strong lensing statistics as a tool to test cosmological models, a detailed account of possible systematic effects is required. Here we provide a brief discussion of some effects and how to quantify them.

One of the most important systematic effect is the magnification bias (Turner et al. 1984). It affects magnitude limited surveys, since gravitationally lensed sources are preferentially included in the survey. This bias may be quite large, depending on the quasar luminosity function. Other important biases are the selection effects due to the limitations on the dynamical range (magnitude differences between the lensed images), resolution limitations and the presence of confusing sources such as stars (Kochanek 1991, 1993a). Besides these there is the issue of selection effects associated with quasar surveys (which tends to misrepresent the quasar population) such as the luminosity of the lensing galaxy (which tends to overwhelm the quasar luminosity and exclude it from the catalogue) and the reddening due to the lensing galaxy (which may reduce the average magnification bias, increase flux ratios and absorb single images) (Kochanek 1991).

Effects due to the lensing galaxy luminosity are expected to be marginal for bright quasar surveys, but for deep (low luminosity cut-off) surveys such as the SDSS the effect might be statistically dominant. Following Cooray & Hutterer (1999), we shall not include this correction. A correct estimate of these effects requires an accurate characterization of the apparent magnitudes of lensing galaxies as function of redshift (Kochanek 1991). Since there still is no consensus on how to quantify the reddening effect (Malhotra, Rhoads, & Turner 1997; Falco, Kochanek, & Muñoz 1998), we shall follow, as before, Cooray & Hutterer (1999) and disregard this effect too.

The effect of confusing sources should be negligible if the lensing survey magnitude range is not excessively large ($\Delta m \gtrsim 2.5$ for a survey with $M_{lim} = 20$ mag) (Kochanek

1993a). Thus, we shall disregard corrections of this nature, but remark that the necessity of including this correction depends on the survey characteristics.

All these effects are somewhat connected, especially the magnitude bias, angular separation and dynamic range effect (Kochanek 1993a,b), but since we are considering a hypothetical survey, we do not need to consider a detailed selection function. Hence we will follow the simplified approach of Cooray (1999), and write the probability that a source at redshift z will be lensed and detected as

$$p(z) = \tau B(< m) f(\Delta\theta) \,, \tag{36}$$

where $B(< m)$ is the average magnification bias for the survey, which will be defined, and $f(\Delta\theta)$ is the angular selection function. Since we found no information on the expected magnitude difference limit for the SDSS we choose just to consider the correction due to the angular resolution. The ignored correction should be small (≈ 0.9997 as estimated in Cooray (1999) for $\Delta m < 2.5$, see also Kochanek (1993a)), hence ignoring this effect will not yield a large error.

Considering the assumptions commonly used in the literature (see, for instance, Fukugita & Turner (1991)), the magnitude bias at a given magnitude level, $B(m)$, is given by

$$B(m) = \frac{1}{N_Q(m)} \int_0^\infty N_Q(m + \Delta) P(\Delta) d\Delta \,, \tag{37}$$

where $N_Q(m)$ is the intrinsic quasar number counts, $\Delta = 2.5 \log \mathcal{A}$, $\mathcal{A}$ being the total magnification produced by the lens, and $P(\Delta) d\Delta$ is the probability distribution of Δ. The probability distribution of the magnification $\mathcal{A}$ is given by (Turner et al. 1984)

$$P(\mathcal{A}) d\mathcal{A} = \frac{8}{\mathcal{A}^3} d\mathcal{A} \qquad \mathcal{A} \geq 2 \,, \tag{38}$$

or alternatively

$$P(\Delta) d\Delta = 7.37 \times 10^{-0.8\Delta} d\Delta \qquad \Delta \geq 0.75 \,. \tag{39}$$

We shall use the quasar number counts from Hartwick & Schade (1990),

$$N_Q(m_b) = \begin{cases} (10/\Box^O) 10^{0.86(m_B - 19.15)} & m_B \leq 19.15 \,, \\ (10/\Box^O) 10^{0.28(m_B - 19.15)} & m_B \geq 19.15 \,. \end{cases} \tag{40}$$

The $\Box^O$ represents the number of sources per square degree of sky. Note that the normalization of the number counts does not influence the magnification bias. The magnification bias is given by (Fukugita & Turner 1991)

$$B(m_B) = \begin{cases} 59.5 \times 10^{0.06(19.15 - m_B)} - 59.2 & m_B \leq 18.40 \,, \\ 2.5 \times 10^{0.58(19.15 - m_B)} & 18.40 < \ m_B < 19.15 \,, \\ 2.50 & m_B \geq 19.15 \,. \end{cases} \tag{41}$$

Since we are working with a hypothetical data set, we must average $B(m)$ over the observed magnitude distribution. The average bias for a survey whose magnitude limit is m_L, $B(< m_L)$, is then

$$B(< m_B) = \frac{\int_{-\infty}^{m_L} N_Q(m_B) B(m_B) dm_B}{\int_{-\infty}^{m_L} N_Q(m_B) dm_B} \ . \tag{42}$$

For the SDSS, Cooray & Hutterer (1999) used a limiting magnitude of $m_L = 21$ mag, although the survey has a limiting magnitude of $m_L = 23$ mag. We shall follow this suggestion and also use $m_L = 21$ mag, which corresponds to an average magnification bias factor of $B(< m_L) = 2.89$.

Moreover we will use a step angular selection function, such that the lens is detected if the angular separation is between $0.1''$ and $6''$, being undetected otherwise. For a SIS model, the fraction of lenses in this range is 0.901 (using the results from Kochanek (1993b); Fukugita & Turner (1991)). We shall consider a simplified selection function such that all lenses within this angular separation range will be recovered and write $f(\Delta\theta) = 0.901$. The angular limits used are very optimistic, but this provides an estimate of how precise the survey must be to obtain sensible results.

Clearly, what is observed in strong gravitational lensing statistics is the fraction of lensed sources relative to the overall number of sources. Consider that N_{Total} sources (such as quasars or galaxies) are found. To study the effect that the size of the survey will have on the precision of the test, we consider three test models, with $N_{Total} = 25000, 10^5, 10^6$ sources (the SDSS survey is expected to yield the spectra of 10^5 quasars, and about 10^6 optical quasars. The 2dF survey expects to find 25000 QSO), spread uniformly in 40 redshift bins of width $\Delta z = 0.1$, starting from $z_{min} = 0$ until $z_{max} = 4$. In this model there will be $n = N_{Total}/40$ sources in each redshift bin. The effect of considering a coarser angular resolution may be seen as having less sources at each redshift. Thus, the 10^6 case may be seen as the best scenario. A more realistic angular selection function would give results that are between the 10^5 and the 10^6 sources cases.

Consider now a fixed redshift bin z_i. For this redshift bin $n = N_{Total}/40$ sources are picked, each one with an independent probability of being lensed given by $p(z_i)$. The number of lensed sources with redshift z_i, $N_L(z_i)$, is then a binomial random variable with parameters n and $p(z_i)$. Since n is large, and $p(z_i)$ is very small, one may use the Poisson PDF with average

$$N_{exp}(z_i) = np(z_i) \ . \tag{43}$$

4.3. Building Confidence Regions.

In order to build up confidence regions we employ the Fisher information matrix method (see e.g. Tegmark, Taylor, & Heavens (1997)), which provides an estimate of the inverse covariance matrix when the likelihood function of the random variable is known.

The Fisher matrix F is given by:

$$F_{ij} = -\left\langle \frac{\partial^2 \ln L}{\partial \theta_i \partial \theta_j} \right\rangle_{\mathbf{x}} \tag{44}$$

where L is the likelihood of observing the data set $\mathbf{x}$ given the parameters $\theta_1, \ldots, \theta_\nu$, and the average is being computed at the point corresponding to the true set of parameters $\mathbf{\Theta}_{true}$. The Fisher information matrix is the expectation value of the inverse of the covariance matrix at the maximum likelihood point, and it gives us a measure of how fast (on average) the likelihood function falls off around the maximum likelihood point. Assuming the Poisson statistics as a good description of the expected number of lenses as function of redshift, the likelihood function is written as

$$L[n_L(\Delta z_1), n_L(\Delta z_2), ..., n_L(\Delta z_{max})] =$$
$$= \prod_{z=0}^{z_{max}} \frac{e^{-N_{exp}(\Delta z_i)} N_{exp}^{n_L(\Delta z_i)}}{n_L(\Delta z_i)!} . \tag{45}$$

Taking the logarithm and calculating the derivatives one obtains (Cooray & Hutterer 1999)

$$F_{ij} = \sum_{\Delta z} \frac{1}{N_{exp}(z, \Delta z)} \frac{\partial N_{exp}(z, \Delta z)}{\partial \theta_i} \frac{\partial N_{exp}(z, \Delta z)}{\partial \theta_j} . \tag{46}$$

Confidence regions are built by imposing a confidence limit on the likelihood function. To build these regions using the Fisher matrix one starts by expanding the logarithm of the likelihood in a Taylor series around the maximum likelihood point. Since this corresponds to a maximum of L, the first derivative vanishes and one finds

$$2\ln(L_{max}/L) = \delta\boldsymbol{\theta} F \delta\boldsymbol{\theta} , \tag{47}$$

where $\delta\boldsymbol{\theta} = (\theta_1 - \theta_{1,max}; ...; \theta_\nu - \theta_{\nu,max})$. By choosing a range of values of $2\ln(L_{max}/L)$ corresponding to the desired confidence level, a second order equation in the $\delta\theta_i$ is obtained which can be solved to obtain the desired confidence regions. It can be shown that in the large n limit, $2\ln(L_{max}/L)$ has a χ^2 distribution with ν degrees of freedom (Kochanek 1993b). For our study $\nu = 2$, and the 68.3%CL are found by imposing $2\ln(L_{max}/L) = 2.3$, while the 95%CL regions are found by imposing $2\ln(L_{max}/L) = 5.99$.

It should be pointed out that this population model is not very realistic since fewer sources are found at low redshift due to the smaller volume involved and, on the other hand, fewer sources at high redshift as only very bright sources are visible. Considering a more realistic distribution should not change the results appreciably though, as one finds more sources at the medium redshift range, thus with a higher lensing rate, but on the other, fewer sources are found at high redshift, which results in an overall lower lensing rate. These two competing effects should thus cancel each other, and produce a small net effect.

4.4. Results.

The confidence regions that were built are shown in Figures 4-8. Since their implications are quite different, the results for each fiducial model are analysed separately. We consider strong lensing statistics as probe by themselves, and together with CMBR peak location and SNAP constraints. This goes beyond the analysis of Makler et al. (2002) where only the SNAP data was considered, and the analysis of Bento et al. (2002b, 2003), where only the CMBR peak location was analised.

4.4.1. Model I.

The gravitational lensing statistics test by itself is unable to yield important constraints on the parameter space of the GCG model, and, at most allows asserting that $0.76 \lesssim A_s \lesssim 0.94$, with no limits on α. Even considering the CMBR peak position data from Archeops and BOOMERANG only an upper value $\alpha \lesssim 0.7$, and $0.76 \lesssim A_s \lesssim 0.87$ is found, as can be seen in Figure 4.

Thus, combining CMBR constraints from Bento et al. (2002b), lensing statistics and SNAP data (Figure 5) does not improve the limits found in Section 3.4. There is only a marginal improvement in the upper range of the allowed values of α. Therefore it is expected that, if the limits imposed in Bento et al. (2002b) are accurate, SNe distance measurements and strong gravitational lensing statistics we will not be able to substantially improve the present constraints, at least in the near future.

4.4.2. Model II.

For the second fiducial model, the results are more promising. As may be seen in Figure 6, the search for lenses in the SDSS will allow to impose a fairly tight parameter range

$\alpha \lesssim 0.3$, and $0.75 \lesssim A_s \lesssim 0.85$. For smaller lens surveys, these results together with CMBR peak location data may yield some constraints. It is particularly interesting to note that a survey with the size of the 2dF survey might be able to place some interesting upper limits on A_s and α in the very near future, although it should be realized that using a more careful treatment of the selection effects might broaden the confidence regions.

The most interesting results appear when we use both SNAP data and lensing statistics for a large survey such as the SDSS (Figures 7 and 8). We are close to determining the model, as they will allow to constrain the parameters to be in the range $\alpha \lesssim 0.1$ and $0.75 \lesssim A_s \lesssim 0.77$ at 68% CL, or $\alpha \lesssim 0.2$ and $0.75 \lesssim A_s \lesssim 0.79$ at 95% CL. This means that SNAP data together with strong lensing statistics from a large precise survey should be able to rule out the CGC model as an unification scheme between dark matter and dark energy.

4.5.   Conclusions and Outlook.

In this paper we have studied how the SNAP data and the data from future quasar surveys might be used to constrain a generalized Chaplygin equation of state. Our conclusions depend on the models under consideration.

If the fiducial model is the model favored by available SNe (Makler et al. 2002), CMBR peak location (Bento et al. 2002b) and age estimates of distance sources (Alcaniz et al. 2002) (Model I in Table 2), then the SNAP data will be able to definitely rule out both the pure Chaplygin case, as well as the ΛCDM model, but it will not be able to provide tighter constraints than those already available. This is particularly so without a precise determination of the Hubble constant, H_0, and of the SNe absolute magnitudes, M in Eq. (22). In fact, to completely rule out the ΛCDM model, a good determination of these quantities is absolutely required.

Using the available data on the CMBR peaks positions from BOOMERANG (de Bernardis et al. 2002) and from Archeops (Benoit et al. 2002), a slight improvement in the allowed parameter range is expected, but most likely to verify the range of parameters determined in Bento et al. (2002b), namely $0.81 \lesssim A_s \lesssim 0.85$ and $0.2 \lesssim \alpha \lesssim 0.65$ at 68% CL, or $0.15 \lesssim \alpha \lesssim 0.75$ and $0.79 \lesssim A_s \lesssim 0.87$ at 95% CL. Of course that the situation will improve greatly with data from WMAP, especially with a more precise determination of the location of the acoustic peaks (Bento et al. 2002b).

Lensing statistics by themselves will not be very helpful in constraining the allowed range of parameters, but together with SNAP data and CMBR constraints, the allowed parameter range is slightly tighter, yielding $0.81 \lesssim A_s \lesssim 0.85$, and $0.2 \lesssim \alpha \lesssim 0.6$ at 68% CL.

We therefore conclude that in order to achieve more precise limits on our fiducial Model I, the best strategy is to aim for better determinations on the location of the CMBR acoustic peaks. If the Universe is best described by Model I, the data from SNAP or from the search for lenses in large quasar surveys will only be able to verify the present day limits, and only marginally to improve them.

Turning now to the ΛCDM fiducial model (Model II in Table 2), the results are much better. Again, an accurate determination of the zero point $\mathcal{M}$ is required in order to achieve some precision. With such a determination one might rule out models with $\alpha \gtrsim 0.2$ at 68% CL, or with $\alpha \gtrsim 0.35$ at 95% CL. Using the CMBR peaks locations, marginal improvements may be obtained. The best results arise from the use of SNe and lensing statistics, where one comes close to determining the model, obtaining the allowed range, $\alpha \lesssim 0.1$ and $0.75 \lesssim A_s \lesssim 0.77$ at 68% CL, and $\alpha \lesssim 0.2$ and $0.75 \lesssim A_s \lesssim 0.79$ at 95% CL. The lensing results should be regarded with care, since our best case scenario is overtly optimistic.

Therefore, if one considers a two component Universe made up of baryons and the GCG, future data from SNAP and from large QSO surveys, such as the SDSS, will be able to test the GCG model, and rule out a possible unification scheme between dark energy and dark matter it provides. The question of how well we will be able to constrain the parameter space depends on the model that is ruled out.

4.5.1. Assumptions made for strong lensing statistics.

As a final note, we mention that caution should be exerted when considering results from gravitational lensing statistics, as there are several systematic effects that we have not explored. The inclusion of a core radius on the galaxy model, for instance, will greatly suppress the lensing optical depth (Hinshaw & Kraus 1987), but on the other hand it will enhance the magnification bias (Kochanek 1996). This partly compensates the lower lensing probability and produces a small net effect. Also, the lack of central images in observed gravitational lenses indicates that the core radii will be smaller than 200 pc (Wallington & Narayan 1993). These results also agree with Kochanek (1996), and Fukugita & Turner (1991) where strong lensing statistics were used to constrain several systematic uncertainties. Therefore, the error from ignoring the core radius appears to be negligible. However, since one is dealing with an unprecedented degree of precision, uncertainties will inevitably affect the results.

Effects due to galactic evolution have been studied in Mao (1991), Mao & Kochanek (1994),and Rix et al. (1994), with the conclusion that evolution will only affect the statistics

substantially if it is important at $z \lesssim 1$. For a vacuum dominated Universe this should not be a problem since galaxies form earlier that for a matter dominated Universe (Carrol, Press, & Turner 1992). Still, evolutionary studies of galaxies have not reached conclusive results. For instance, results from the Canada-France Survey (Lilly et al. 1995) indicate that the comoving number density of sources is independent of redshift. On the other hand, results from the Hubble Deep Field depend on the methods used to estimate the redshift distribution of sources. In Mobasher et al. (1996) it is argued that there are no signs of evolution, while Sawicki, Lin, & Yee (1997) indicate that there is some evolution, although not a dramatic one, from $0.2 < z < 0.5$ until $1 < z < 2$. On the other hand, a more dramatic evolution from $z = 2.2$ until $z = 0.6$ is argued in Gwyn & Hartwick (1996).

In calculating the parameter F in Eq. (34), we must relate the velocity dispersion of matter in the galaxy to its luminosity. The problem of estimating the dark matter velocity dispersion σ_{DM} from the luminous matter in elliptical galaxies arises, and is of great importance in gravitational lensing statistics, since a 22% change of $\sigma_{\parallel}$ in Eq. (34) leads to a 125% change in the expected number of lenses and a 50% change in image separations. Here we assumed that the velocity dispersion of dark matter is the same as the luminous matter, as considered in Kochanek (1991, 1993a,b, 1996), Chiba & Yoshii (1999), Cooray (1999), Cooray & Hutterer (1999), and Cooray, Quashnock, & Miller (1999). This equality was advocated in Kochanek (1993b) and Kochanek (1996). Other studies have suggested that a correction of order $(3/2)^2$ should be included in the dark matter velocity dispersion (Turner et al. 1984). This correction is most likely inaccurate since it was computed using the global virial theorem, which is not valid for power law profiles that diverge at the origin or at infinity. Fitting the observed velocity dispersion as function of radius to tracer models of the isothermal sphere profile, it was concluded that $\sigma_{DM} \sim v_{los}$ for regions close to the center of the galaxies (Kochanek 1993b). This was verified by lensing statistics also, in Kochanek (1994). This conclusion is also supported by detailed dynamical modeling of early type galaxies (Breimer & Sanders 1993; Franx 1993; Kochanek 1994). There is also a 30% uncertainty in the value of F, which we did not take into account. This uncertainty is likely to become smaller once more data on galaxies become available.

In our estimates, effects such as reddening and the luminosity of the lensing galaxy (Kochanek 1991) were ignored as there is still not enough quantitative knowledge of their results, but it is known that for a faint survey, such as the SDSS, effects due to the luminosity of the lensing galaxy must be taken into account.

REFERENCES

Albrecht, A., & Skordis, C. 2000, Phys. Rev. Lett., 84, 2076

Alcaniz, J. S., Jain, D., & Dev, A. 2002, Phys. Rev. D, in press (astro-ph/0210476)

Alcock, C., & Paczynski, B. 1979, Nature, 281, 358

Amendola, L. 1999, Phys. Rev. D, 60, 043501

Avelino, P. P., Beça, L. M. G., de Carvalho, J. P. M., Martins, C. J. A. P., & Pinto, P. 2002, Phys. Rev. D, 67, 023511

Bahcall, N. A., & Fan, X. 1998, ApJ, 504, 1

Balbi, A., et al. 2000, ApJ, 545, L1

Banerjee, N., & Pavón, D. 2001a, Phys. Rev. D, 63, 043504

Banerjee, N., & Pavón, D. 2001b, Class. Quantum Gravity, 18, 593

Bean, R., & Doré, O., preprint (astro-ph/0301308)

Beça, L.M.G., Avelino, P.P., de Carvalho, J.P.M., Martins, C.J.A.P., preprint (astro-ph/0303564)

Benoit, A., et al. 2002, A&A, in press (astro-ph/0210306)

Bento, M. C., & Bertolami, O. 1999, Gen. Relativity and Gravitation, 31, 1461

Bento, M. C., Bertolami, O., & Rosenfeld, R. 2001, Phys. Lett. B, 518, 276

Bento, M. C., Bertolami, O., & Santos, N. C. 2002, Phys. Rev. D, 65, 067301

Bento, M. C., Bertolami, O., & Sen, A. A. 2002a, Phys. Rev. D, 66, 043507

Bento, M. C., Bertolami, O., & Sen, A. A. 2002b, Phys. Rev. D, 67, 063003

Bento, M. C., Bertolami, O., & Sen, A. A. 2003, preprint (astro-ph/0303538)

Bento, M. C., Bertolami, O., & Silva, P. T. 2001, Phys. Lett. B, 498, 62

Bertolami, O. 1986a, Il Nuovo Cimento, 93B, 36

Bertolami, O. 1986b, Fortschr. Physik, 34, 829

Bertolami, O., & Martins, P. J. 2000, Phys. Rev. D, 61, 064007

Bilić, N., Tupper, G. B., & Viollier, R. D. 2002, Phys. Lett. B, 535, 17

Binétruy, P. 1999, Phys. Rev. D, 60, 063502

Breimer, T. G., & Sanders, R. H. 1993, A&A, 274, 96

Bronstein, M. 1933, Phys. Zeit. Soweijt Union, 3, 73

Burles, S., Nollet, K. M., & Turner, M. S. 2001, ApJ, 552, L1

Caldwell, R. R., Dave, R., & Steinhardt, P.J. 1998, Phys. Rev. Lett., 80, 1582

Carlberg, R. G., Yee, H. K. C., Morris, S. L., Lin, H., Ellingson, E., Patton, D., Sawicki, M., & Shepherd, C. W. 1999, ApJ, 516, 552

Carrol, S. M., Press, W. H., & Turner, E. L. 1992, ARA&A, 30, 499

Chiba, T. 1999, Phys. Rev. D, 60, 083508

Chiba, M., & Yoshii, Y. 1999, ApJ, 510, 42

Cooray, A. R. 1999, A&A, 342, 353

Cooray, A. R., & Huterer, D. 1999, ApJ, 513, L95

Cooray, A. R., Quashnock, J. M., & Miller, M. C. 1999, ApJ, 511, 562

de Bernarbis, P., et al. 2000, Nature, 404, 955

de Bernardis, P., et al. 2002, ApJ, 564, 559

Dev, A., Alcaniz, J. S., & Jain, D. 2002, Phys. Rev. D, 67, 023515

Falco, E. E., Kochanek, C. S., & Muñoz, J. A. 1998, ApJ, 494, 47

Ferreira, P. G., & Joyce, M. 1998, Phys. Rev. D, 58, 023503

Franx, M. 1993, in Galactic Bulges, ed. H. Dejonghe & H.J. Habing (Dordrecht:Kluwer), 243

Fujii, Y. 2000, Phys. Rev. D, 62, 064004

Fukugita, M., & Turner, E. L. 1991, MNRAS, 253, 99

Garnavich, P. M., et al. 1998, ApJ, 509, 74

Goliath, M., Amanullah, R., Astier, P., Goobar, A., & Pain, R. 2001, A&A, 380, 6

Gott, J. R., Park, M., & Lee, H. M. 1989, ApJ, 338, 1

Gwyn, S. D. J., & Hartwick, F. D. A. 1996, ApJ, 468, L77

Hartwick, F. D. A., & Schade, D. 1990, ARA&A, 28, 437

Hinshaw, G., & Krauss, L. M. 1987, ApJ, 320, 468

Jaffe, A. H., et al. 2001, Phys. Rev. Lett., 86, 3475

Kamenshchik, A., Moschella, U., & Pasquier, V. 2001, Phys. Lett. B, 511, 265

Kim, J. E. 1999, JHEP, 05, 022

Kochanek, C. S. 1991, ApJ, 379, 517

Kochanek, C. S. 1993a, ApJ, 417, 438

Kochanek, C. S. 1993b, ApJ, 419, 12

Kochanek, C. S. 1994, ApJ, 436, 56

Kochanek, C. S. 1996, ApJ, 466, 638

Lilly, S. J., Le Fèvre, O., Crampton, D., Hammer, F., & Tresse, L. 1995, ApJ, 455, 50

Makler, M., Oliveira, S. Q., & Waga, I. 2002, Phys. Lett. B, 555, 1

Malhotra, S., Rhoads, J. E., & Turner, E. L. 1997, MNRAS, 288, 138

Mao, S. 1991, ApJ, 380, 9

Mao, S., & Kochanek, C. S. 1994, MNRAS, 268, 569

Masiero, A., Pietroni, M., & Rosati, F. 2000, Phys. Rev. D, 61, 023504

Mobasher, B., Rowan-Robinson, M., Georgakakis, A., & Eaton, N. 1996, MNRAS, 282, L7

Ozer, M., & Taha, M. O. 1987, Nucl. Phys. B, 287, 776

Peacock, J. A., et al. 2001, Nature, 410, 169

Perlmutter, S., et al. 1997, ApJ, 483, 565

Permutter, S., et al. 1998, Nature, 391, 51

Perlmutter, S., et al. 1999, ApJ, 517, 565

Ratra, B., & Peebles, P. J. E. 1988a, ApJ, 325, L117

Ratra, B., & Peebles, P. J. E. 1988b, Phys. Rev. D, 37, 3406

Reis, R.R.R., Waga, I., Calvão, M.O., Jorás, S.E., astro-ph/0306004

Riess, A. G., et al. 1998, AJ, 116, 1009

Rix, H., Maoz, D., Turner, E. L., & Fukugita, M. 1994, ApJ, 435, 49

Sandvik, H., Tegmark, M., Zaldarriaga, M., Waga, I., astro-ph/0212114

Sawicki, M. J., Lin, H., & Yee, H. K. C. 1997, AJ, 113, 1

Sen, A. A., & Sen, S. 2001, Mod. Phys. Lett.A, 16, 1303

Sen, A. A., Sen, S., & Sethi, S. 2001,Phys. Rev. D, 63, 107501

Spergel, D. N., et al. 2003, ApJ, submitted

Tegmark, M., Taylor, A. N., & Heavens, A. F. 1997, ApJ, 480, 22

Turner, E. L., Ostriker, J. P., & Gott, J. R. 1984, ApJ, 284, 1

Turner, M. S. 2000, Phys. Scr, T85, 210

Uzan, J. P. 1999, Phys. Rev. D, 59, 123510

Wallington, S., & Narayan, R. 1993, ApJ, 403, 517

Weller, J., & Albrecht, A. 2002, Phys. Rev. D, 65, 103512

Wetterich, C. 1988, Il Nuovo Cimento, B302, 668

Zlatev, I., Wang, L., & Steinhardt, P. K. 1999, Phys. Rev. Lett., 82, 896

Table 1: SNAP specifications for a two year period of observations.

Redshift Interval	z=0-0.2	z=0.2-1.2	z=1.2-1.4	z=1.4-1.7
Number of SNe	50	1800	50	15

Table 2. Parameters for the considered fiducial models.

	Ω_b	Ω_{ch}	A_s	α
Model I	0.05	0.95	0.83	0.4
Model II	0.05	0.95	0.758	0.0
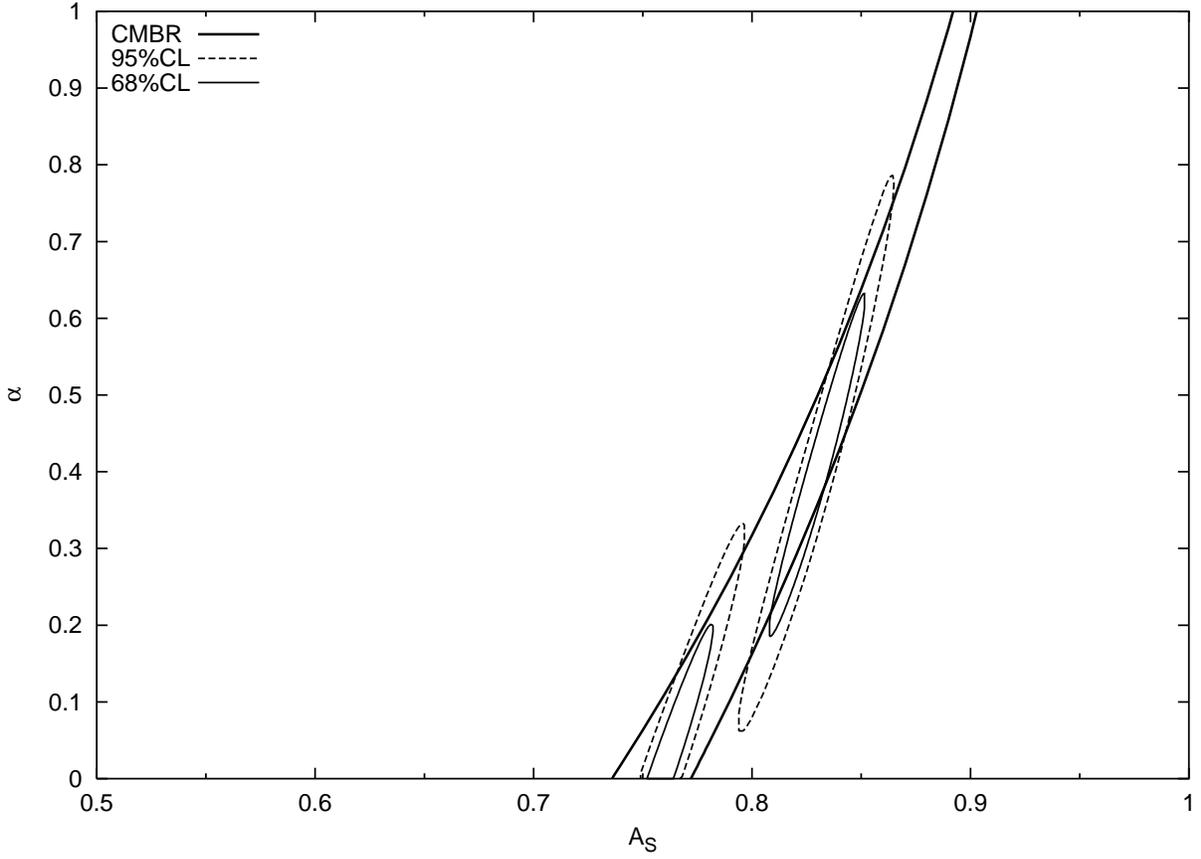
Fig. 1.— Expected SNAP confidence regions assuming precise knowledge of $\mathcal{M}$ plus the CMBR constraints from Bento et al. (2002b).
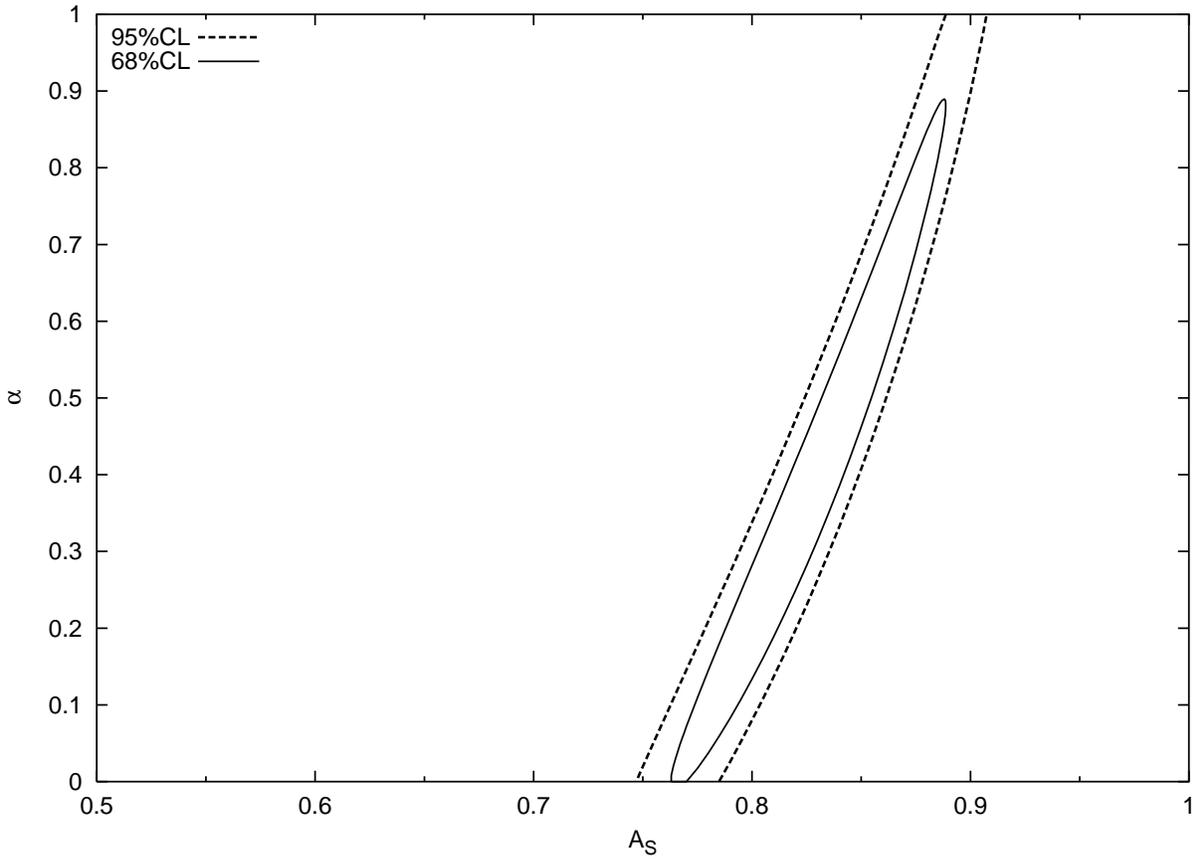
Fig. 2.— Expected SNAP confidence regions for Model I assuming no knowledge of $\mathcal{M}$.
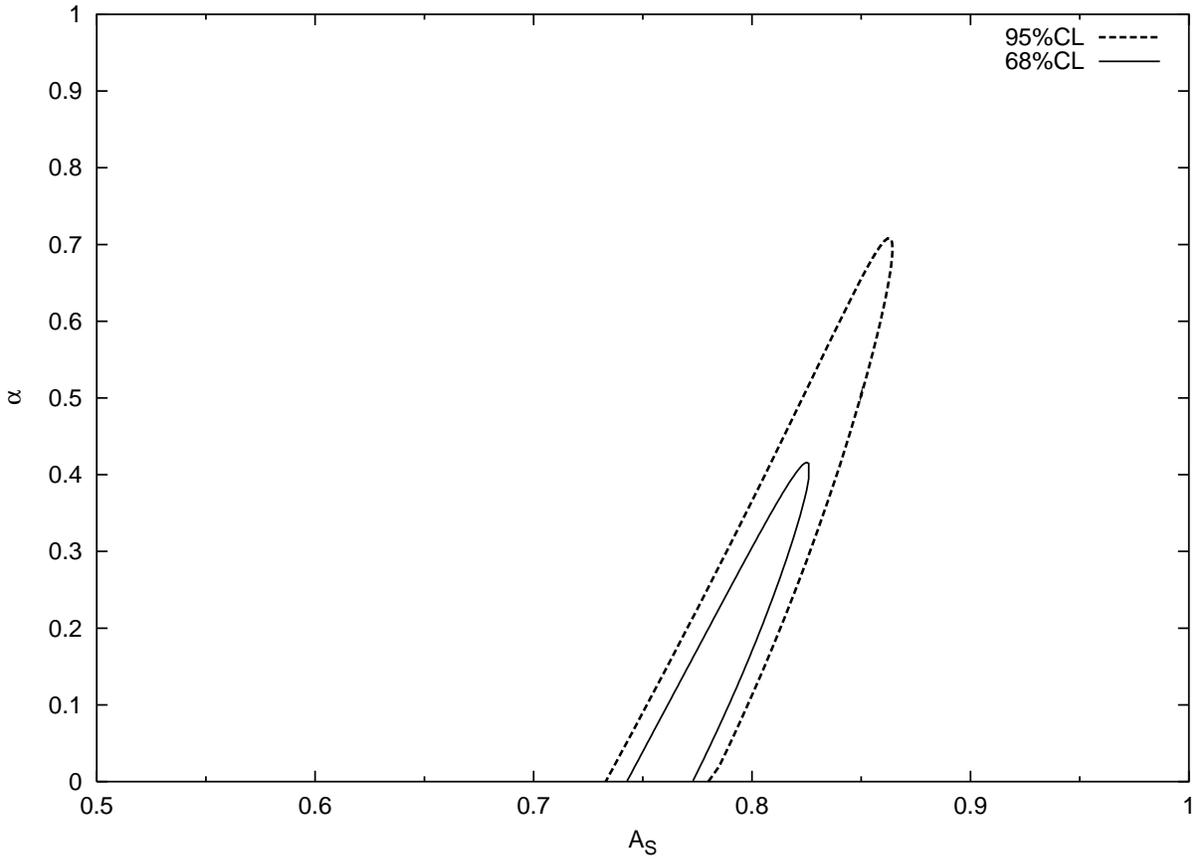
Fig. 3.— Expected SNAP confidence regions for Model II assuming no knowledge of $\mathcal{M}$.
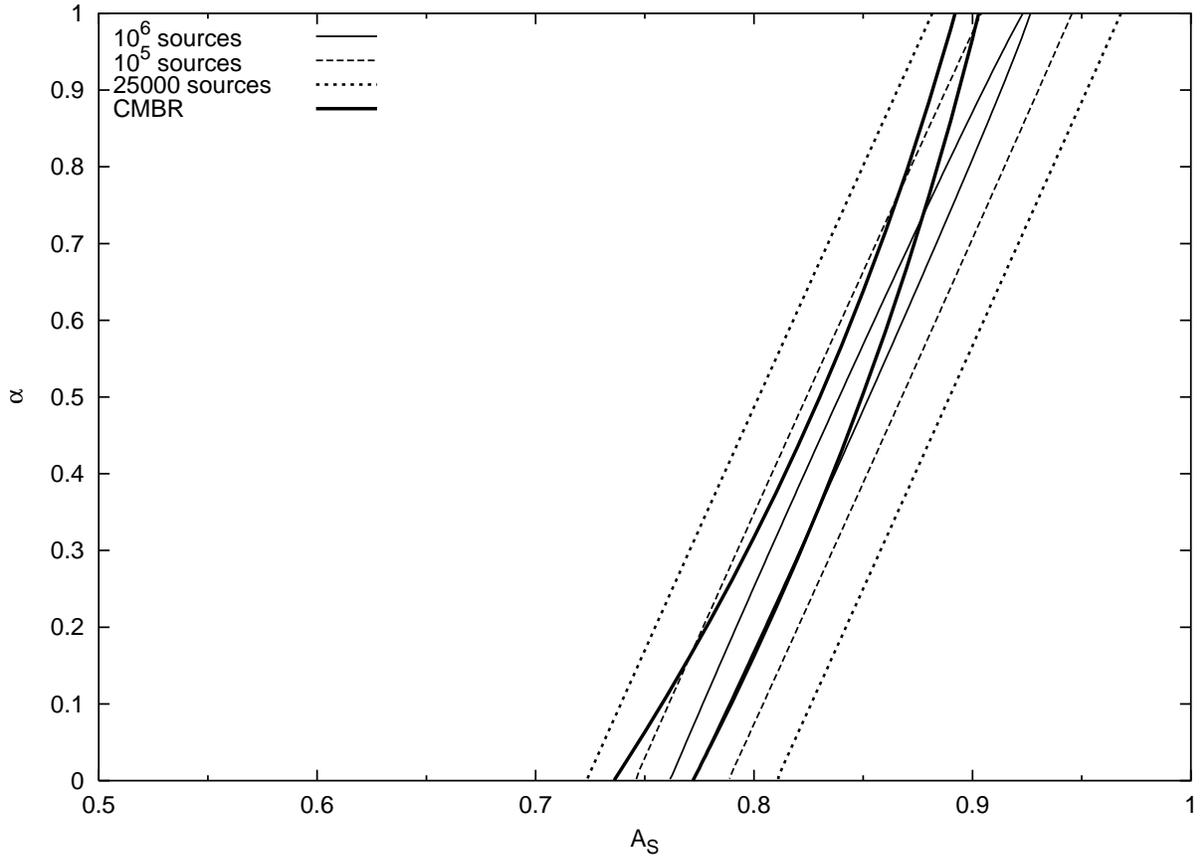
Fig. 4.— Lensing 68% confidence regions for Model I. The thick lines are the CMBR constraints from Bento et al. (2002b).
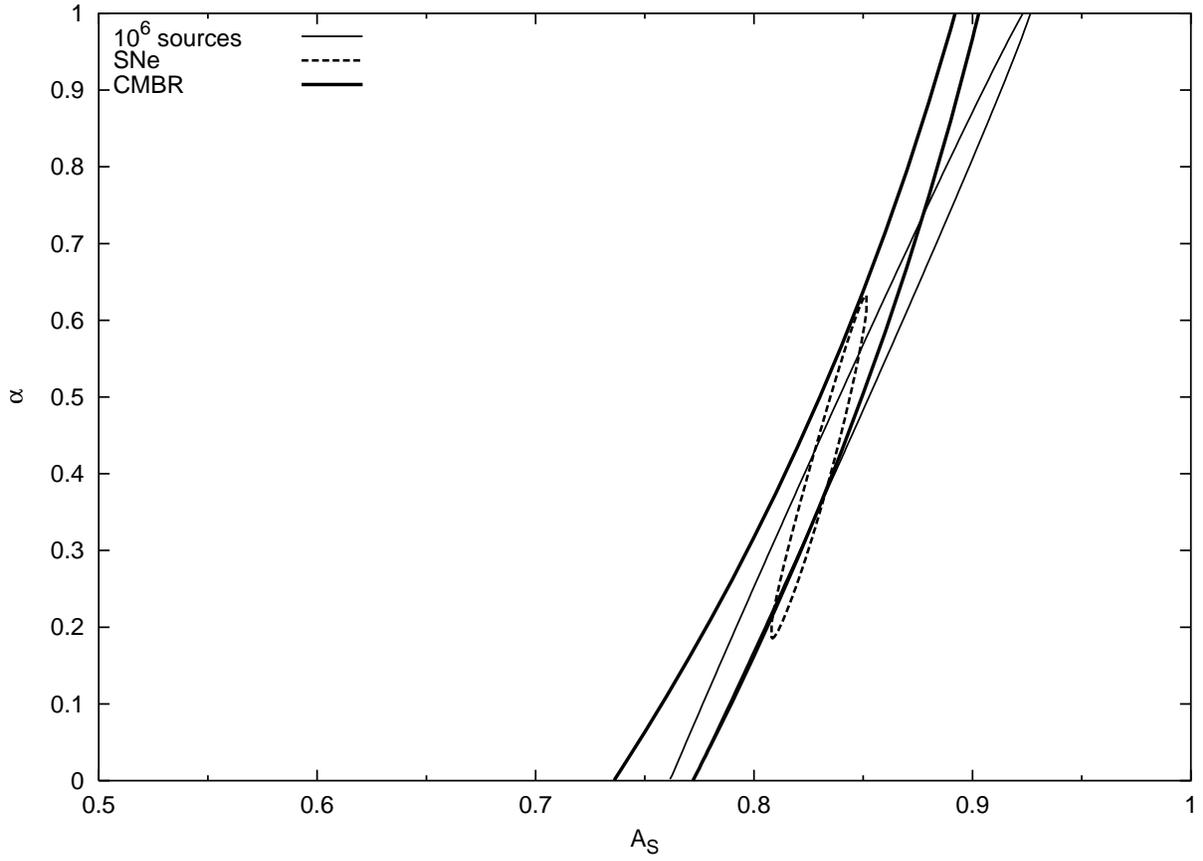
Fig. 5.— Joint 68% confidence regions for Model I from lensing, SNe and CMBR constraints from Bento et al. (2002b). The SNe confidence region is computed assuming an exact $\mathcal{M}$
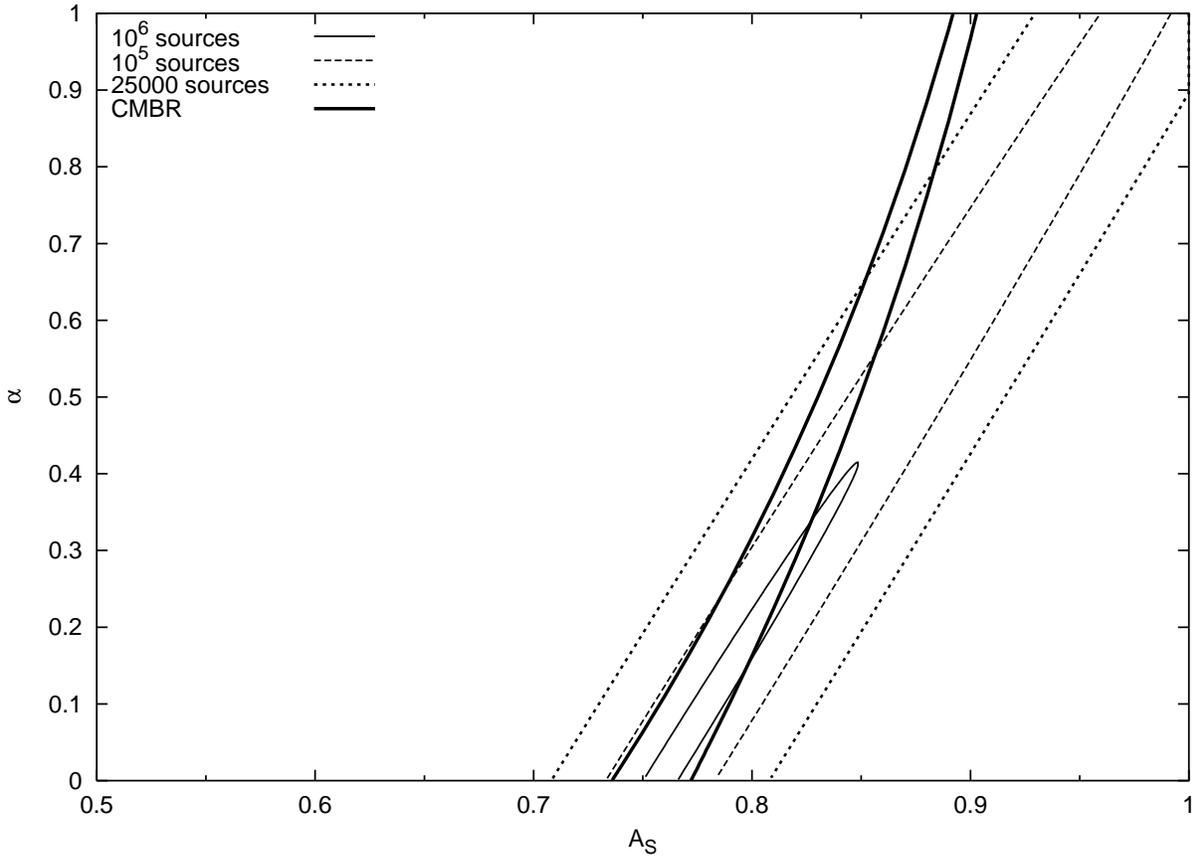
Fig. 6.— Lensing 68% confidence regions for Model II. The thick lines are the CMBR constraints from Bento et al. (2002b).
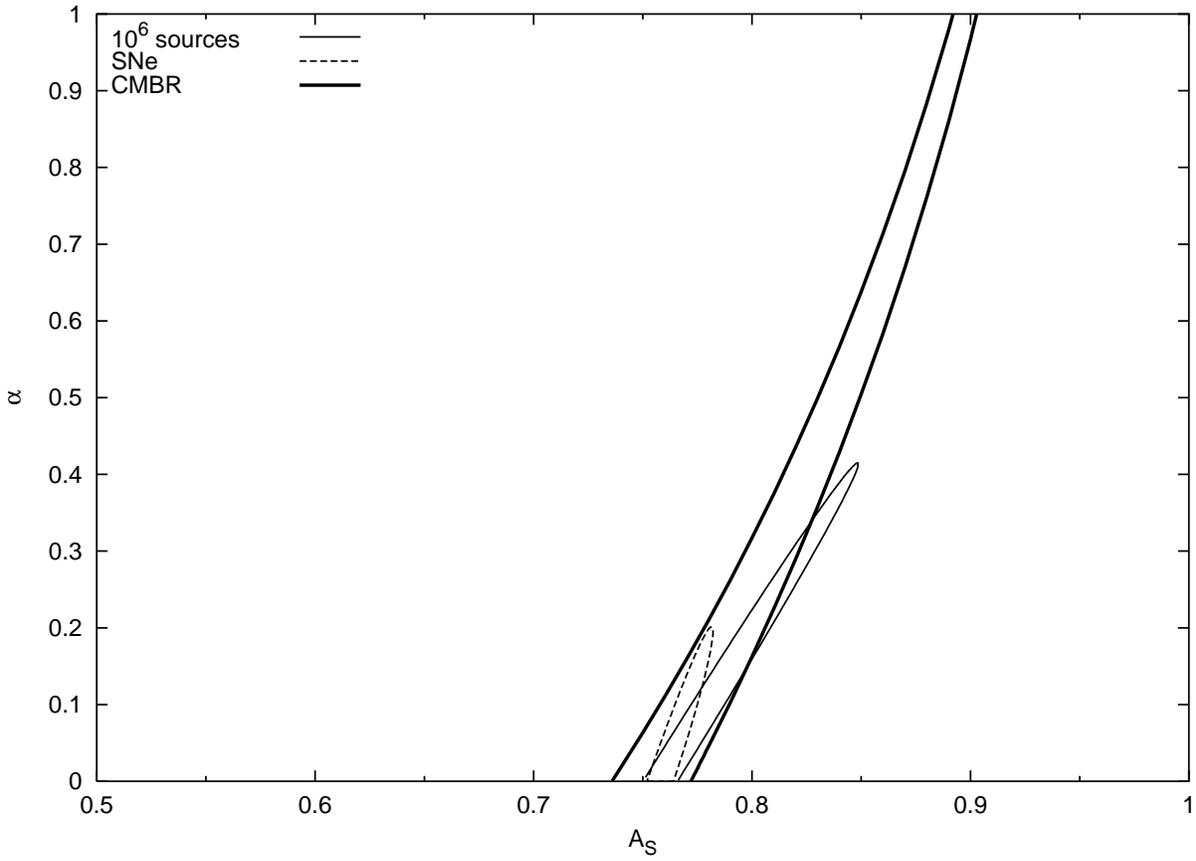
Fig. 7.— Joint 68%CL confidence regions for Model II using both SNe, gravitational lensing statistics and CMBR constraints from Bento et al. (2002b). The SNe confidence region is computed assuming an exact $\mathcal{M}$
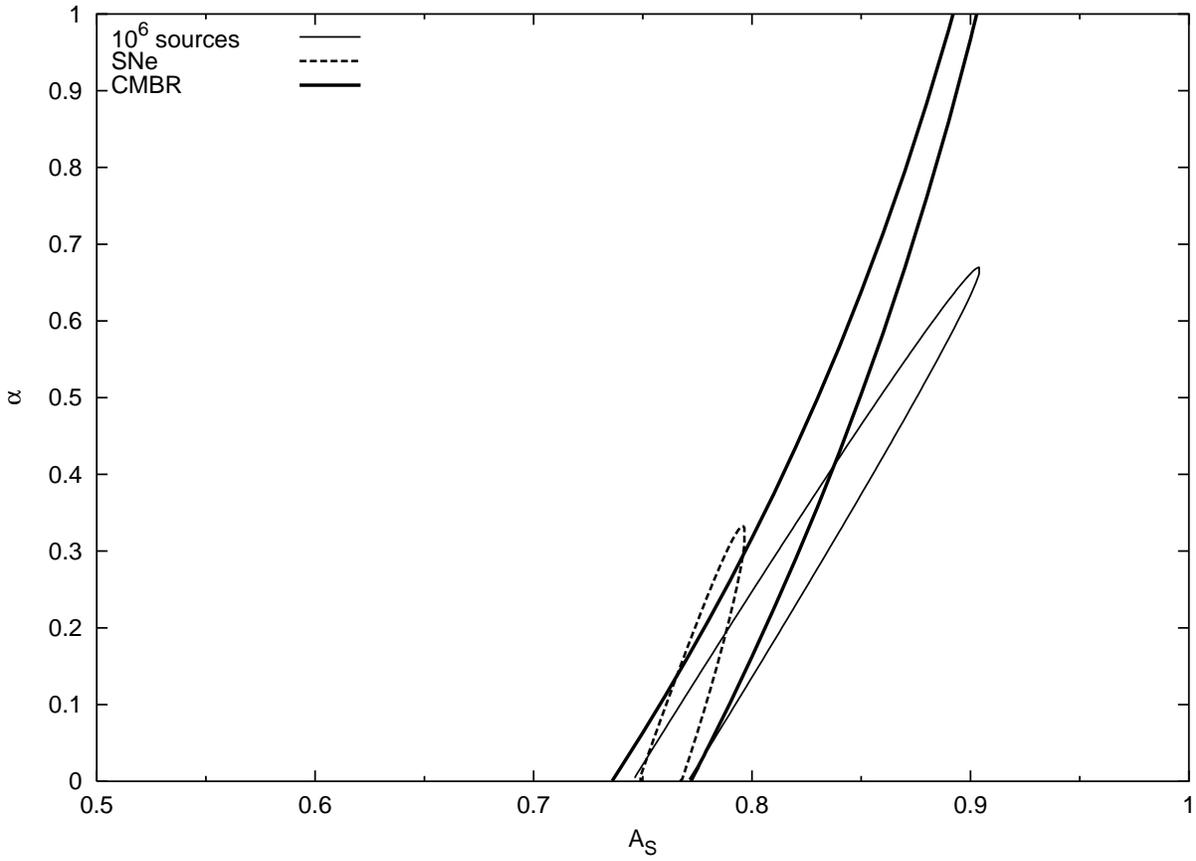
Fig. 8.— Joint 95%CL confidence regions for Model II using both SNe, gravitational lensing statistics and CMBR constraints from Bento et al. (2002b). The SNe confidence region is computed assuming an exact $\mathcal{M}$